

An analytical second-order description of the S_0/S_1 intersection seam: fulvene revisited

Fabrizio Sicilia · Michael J. Bearpark ·
Lluís Blancafort · Michael A. Robb

Received: 10 January 2007 / Accepted: 1 March 2007 / Published online: 26 May 2007
© Springer-Verlag 2007

Abstract A comprehensive picture of the extended S_0/S_1 intersection seam of fulvene is presented, using a complete second-order description. We are now able to discuss the connectivity of all of the seam critical points using the eigenvectors of the intersection-space Hessian. The conjecture (Deeb et al. in Chem Phys 325:251, 2006) that there are two disjoint S_0/S_1 conical intersections seams in fulvene is found to be incorrect. Previously reported high symmetry planar and perpendicular structures are shown to be second-order saddle points on the intersection seam. In addition, the pyramidalized planar structure is shown to be a first-order saddle point, a previously located low symmetry structure is also shown to be a saddle point, and a new global intersection minimum has been found. The local topology (sloped vs. peaked) of these five seam critical points is analysed and interpreted using the second-order analysis.

Keywords Fulvene · Conical intersection · Crossing seam

This paper is dedicated to the memory of Fernando Bernardi who was a collaborator for some 30 years. Our first study of fulvene was carried out with Fernando in 1996.

F. Sicilia · M. J. Bearpark (✉) · M. A. Robb (✉)
Department of Chemistry, Imperial College,
London SW7 2AZ, UK
e-mail: m.bearpark@imperial.ac.uk

M. A. Robb
e-mail: mike.robb@imperial.ac.uk

L. Blancafort
Institut de Química Computational and Departament de Química,
Universitat de Girona, 17071 Girona, Spain

1 Introduction

Conical intersections are often invoked in the rationalization of chemical processes where the pathway involves more than a single potential energy surface (see for example [1–15] and references therein). Conical intersections are not isolated points, but rather they are connected within a $(3N-8)$ -dimensional space (N is the number of atoms) where the degeneracy between the two intersecting states is retained, i.e., the *intersection space* [16]. It is also common to refer to this intersection space as the *crossing hyper-line* (see for instance [3–10]) or the *seam space* (see [1, 2, 14] and references therein). Perpendicular to the intersection space, there exists a two-dimensional complementary space where the degeneracy between the two crossing potential energy surfaces is always lifted, i.e., the *branching space* [16] corresponding to the co-ordinates of the classical funnel.

In most applications involving conical intersections, the two potential energy surfaces in the neighbourhood of a crossing point have been explored mainly using the *first-order approximation* (see for example [1–10]), i.e., characterized exclusively using gradients. Within the first-order approximation, the branching space is described as a plane, i.e., the *branching plane* [16] or *g-h plane* (see for example [1, 2, 14]). The intersection space is approximated to first order by a set of $(3N-8)$ vectors perpendicular to this branching plane [1–6, 9, 16]. The tools to locate, optimize and rationalize conical intersection geometries have been implemented within the first-order approximation (see for example [17–20]). However, the study of conical intersection beyond first order can be fruitful (see for example [11–15, 21–26]). We now summarize the type of additional information that can be obtained from a *second-order description* of conical intersections.

The limitation of a first-order description becomes apparent if one takes a finite linear step, within the $(3N-8)$ -dimensional intersection space, from an optimized crossing point (for a more detailed discussion see for example [24–26]). Surprisingly, the degeneracy between the two states is lifted. This lifting of the degeneracy is due to second-order effects. In the more correct second-order description of conical intersections, both the branching space and intersection space are curved (see for example [16, 22–26]) and therefore are conveniently described by a set of curvilinear co-ordinates rather than rectilinear co-ordinates. In such intersection-space curvilinear co-ordinates, the degeneracy between the two intersecting states is correctly retained for a finite step in the intersection space. The Hessian evaluated with respect to these co-ordinates is the *intersection-space Hessian*: at an optimized conical intersection point, the diagonalization of the intersection-space Hessian gives the curvature of the conical intersection hyper-line energy. Thus, one can characterize optimized conical intersection geometries as either minima or saddle points within the intersection space. The curved nature of the conical intersection seam also manifests itself in the fact that the local topology (*sloped* vs. *peaked* [16]) can change along the hyper-line. We will give an analytic characterization of the sloped versus peaked topology and illustrate this in fulvene calculations to be presented below.

A brief aside on curvilinear co-ordinates completes this qualitative discussion. The position of a point in an m -dimensional space may be given as a set of m numbers, i.e., its co-ordinates. When this set of numbers is given with respect to a set of m level curves rather than to a set of m rectilinear axes, the co-ordinates used are said to be *curvilinear*. The evolution of a curvilinear co-ordinate takes place along a curve, whereas a step along a rectilinear co-ordinate yields a displacement along a straight line. In the application studied in this work, the curvilinear co-ordinates are computed as a non-linear combination of the rectilinear *intersection adapted co-ordinates*, routinely used in the study of conical intersections (see for example [1–10, 14, 16]).

Our objective in this paper is to present a comprehensive analysis of the S_0/S_1 fulvene intersection hyper-line. This is important for three reasons. Firstly, we have previously studied this system with a more approximate version of our second-order analysis [26] than is presented in this paper (and in more detail in [24]). Fulvene has proved to be a useful benchmark study for methods that characterize conical intersection topology, and we now have more consistent data. Secondly, the conical intersection of this system had been also studied by other workers (see for example [27, 28]) and we hope to answer some theoretical questions raised by these studies. In particular, in [28], Deeb et al. proposed that the planar and twisted conical intersection points belong to different disjoint S_0/S_1 intersection seams. We show that this

is incorrect. These authors also claimed that the degeneracy along the torsion co-ordinate is only preserved for angles larger than 45° . However, when a constrained optimization in the intersection space is performed [21], a continuous seam of degenerate points can be mapped along all torsion values. They further suggested that the planar conical intersection was involved in a bond breaking process, and we will also show that this is not correct.

Finally, the general description of the complete topology of intersection hyper-lines is of interest chemically. For example, in our early MMVB studies [29] of fulvene, we showed that the non-radiative decay from the S_1 state of fulvene takes place in the planar conical intersection region. Dynamics calculations showed that the deactivation occurs here, away from the lower-energy twisted region of the intersection hyper-line. Thus, the planar conical intersection was clearly a saddle point, although we had no way to demonstrate this at the time, lacking the second-order analysis as presented in this and in previous works [24–26]. The extended nature of the conical intersection has been demonstrated in several other chemical systems (see for example [4, 9, 21–26, 30]). Thus an accurate description of the curvature of the conical intersection seam is useful to rationalize non-adiabatic deactivation processes in general.

2 Theory

In this section we briefly summarize the second-order description of conical intersections recently developed and how the intersection-space Hessian can be computed [24–26]. The presentation included here provides only the key equations obtained in [24]. Other authors have proposed related approaches to describe conical intersections to the second order (see for example [2, 12–14, 22, 23, 31]). However, most of these methods involve mainly fitting procedures, in contrast to our analytical methodology. In order to give a clearer mathematical presentation, we discuss the second-order description of conical intersections in comparison with the second-order description of a single potential energy surface.

We begin by providing a second-order description of a single Born–Oppenheimer potential energy surface. We can construct such a potential energy surface as a Taylor expansion performed around a reference geometry \mathbf{q}_0 :

$$U_{\text{BO}}(\mathbf{q}) = U_{\text{BO}}^{(0)}(\mathbf{q}_0) + U_{\text{BO}}^{(1)}(\mathbf{q}) + U_{\text{BO}}^{(2)}(\mathbf{q}) \quad (1a)$$

where:

$$U_{\text{BO}}^{(1)}(\mathbf{q}) = \sum_{i=1}^{3N-6} \frac{\partial U_{\text{BO}}(\mathbf{q}_0)}{\partial q_i} q_i = \sum_{i=1}^{3N-6} \kappa_i q_i \quad (1b)$$

$$U_{\text{BO}}^{(2)}(\mathbf{q}) = \frac{1}{2} \sum_{i,j=1}^{3N-6} \frac{\partial^2 U_{\text{BO}}(\mathbf{q}_0)}{\partial q_i \partial q_j} q_i q_j = \frac{1}{2} \sum_{i,j=1}^{3N-6} \gamma_{ij} q_i q_j \quad (1c)$$

such that:

$$U_{\text{BO}}(\mathbf{q}) = U_{\text{BO}}^{(0)}(\mathbf{q}_0) + \sum_{i=1}^{3N-6} \kappa_i q_i + \frac{1}{2} \sum_{i,j=1}^{3N-6} \gamma_{ij} q_i q_j \quad (1d)$$

If we now use the normal co-ordinates, Q_i , that diagonalize the Hessian matrix, γ_{ij} , and we assume the reference point to be an equilibrium geometry, we then obtain:

$$U_{\text{BO}}(\mathbf{Q}) = \frac{1}{2} \sum_{i=1}^{3N-6} v_i Q_i^2 \quad (1e)$$

which is the usual expansion of a single potential energy surface in terms of eigenvalues of the Hessian. Thus, the first-order term $U_{\text{BO}}^{(1)}$ vanishes since the gradient of the potential energy, κ , computed at a minimum point is zero. The remaining second-order term is expressed in normal co-ordinates such that v_i represents the force constants related to the Q_i normal co-ordinates. The force constant v_i can be used to evaluate the frequencies of the molecule at a critical point on the potential energy surface. Furthermore, the sign of v_i is the sign of the surface curvature along the Q_i . Thus, v_i indicates whether the optimized geometry is a minimum, a saddle point or a maximum on the potential energy surface. If N is the number of atoms belonging to a molecule, there are zero, m or $(3N-6)$ negative v_i values for a molecular geometry corresponding to a minimum, an m -order saddle point or a maximum, respectively [32]. (To avoid any confusion: we use ‘order’ in this context to indicate the number of directions that lower the energy at a seam critical point, but these directions are all computed explicitly using a second-order—first and second derivatives—representation of the seam itself.)

We now want to briefly present the analogous development for the expansion of the potential energy surfaces around the conical intersection point and the curvature of the conical intersection hyper-line energy. In other words, when we locate a conical intersection critical point, we wish to know whether it is a saddle point or a minimum on the $(3N-8)$ -dimensional intersection hyper-line.

In the case of two electronic states, i.e., *state A* and *state B*, we can expand the potential energy around a point of degeneracy, i.e., a conical intersection, and develop the two-level analogue of Eq. (1). In this case, we obtain a matrix which can be diagonalized to give the two potential energy surfaces of *state A* and *state B*. We have presented a detailed discussion of this process in [24] and other related theoretical treatments can be found in [1, 2, 11–16, 31, 33]. In the present paper, we report only the main ideas.

The two level expansion analogous to Eq. (1) is shown in Eq. (2).

$$\mathbf{W}(\bar{\mathbf{Q}}) = \begin{pmatrix} \kappa_{x_1}^A \bar{Q}_{x_1} + \kappa_{x_2}^A \bar{Q}_{x_2} & \kappa_{x_2}^{AB} \bar{Q}_{x_2} \\ \kappa_{x_2}^{AB} \bar{Q}_{x_2} & \kappa_{x_1}^B \bar{Q}_{x_1} + \kappa_{x_2}^B \bar{Q}_{x_2} \end{pmatrix} + \frac{1}{2} \begin{pmatrix} \sum_{i,j=1}^{3N-6} \gamma_{ij}^A \bar{Q}_i \bar{Q}_j & \sum_{i,j=1}^{3N-6} \eta_{ij}^{AB} \bar{Q}_i \bar{Q}_j \\ \sum_{i,j=1}^{3N-6} \eta_{ij}^{AB} \bar{Q}_i \bar{Q}_j & \sum_{i,j=1}^{3N-6} \gamma_{ij}^B \bar{Q}_i \bar{Q}_j \end{pmatrix} \quad (2)$$

The potential energy constants used in Eq. (2) are defined in Table 1. Notice that we have partitioned the co-ordinate space such that:

$$\bar{\mathbf{Q}} = (\bar{Q}_{x_1}, \bar{Q}_{x_2}) \oplus (\bar{Q}_3, \bar{Q}_4, \dots, \bar{Q}_{3N-6}) \quad (3a)$$

The first set of co-ordinates, $(\bar{Q}_{x_1}, \bar{Q}_{x_2})$, consists of the two co-ordinates spanning the gradient difference vector, Eq. (3b), and the non-adiabatic interstate coupling vector, Eq. (3c).

$$\mathbf{x}_1 \equiv \frac{\partial(E_B - E_A)}{\partial \mathbf{q}} \quad (3b)$$

$$\mathbf{x}_2 \equiv \frac{\partial \langle \phi_A | \hat{H}_e | \phi_B \rangle}{\partial \mathbf{q}} \quad (3c)$$

Distortions along these two co-ordinates lift the degeneracy and these vectors span the *branching plane* [16]. The second set of co-ordinates in Eq. (3a) corresponds to the co-ordinates along the $(3N-8)$ vectors perpendicular to the branching plane. Along this second set of co-ordinates the degeneracy is retained at the first order.

Notice that the diagonal terms of the matrix in Eq. (2) have the same meaning as the symbols used in Eq. (1). Thus the diagonal of this two-level matrix is a second-order expansion of the potential energy surface, completely analogous to Eq. (1). However, the two energies computed in this diagonal expansion are diabatic energies rather than adiabatic energies. Upon addition of the off-diagonal elements κ^{AB}

Table 1 Definition of the potential energy constants ($k = A, B; i, j = x_1, x_2, 3, \dots, 3N - 6$)

First-order potential energy constants		Second-order potential energy constants	
$\kappa_i^k \equiv \left. \frac{\partial \langle \phi_k \hat{H}_e \phi_k \rangle}{\partial \bar{Q}_i} \right _0$	(a)	$\gamma_{ij}^{kk} \equiv \left. \frac{\partial^2 \langle \phi_k \hat{H}_e \phi_k \rangle}{\partial \bar{Q}_i \partial \bar{Q}_j} \right _0$	(e)
$\kappa_i^{AB} \equiv \left. \frac{\partial \langle \phi_A \hat{H}_e \phi_B \rangle}{\partial \bar{Q}_i} \right _0$	(b)	$\eta_{ij}^{AB} \equiv \left. \frac{\partial^2 \langle \phi_A \hat{H}_e \phi_B \rangle}{\partial \bar{Q}_i \partial \bar{Q}_j} \right _0$	(f)
$\lambda_i \equiv \kappa_i^B + \kappa_i^A$	(c)	$\omega_{ij} \equiv \gamma_{ij}^{AA} + \gamma_{ij}^{BB}$	(g)
$\delta\kappa \equiv \kappa_i^B - \kappa_i^A$	(d)	$\delta\gamma_{ij} \equiv \gamma_{ij}^{BB} - \gamma_{ij}^{AA}$	(h)

ϕ_k represents the optimized wave-function of the k th state and \hat{H}_e is the electronic Hamiltonian

and η^{AB} , which represent the expansion of the interaction of the diabatic states, followed by the diagonalization of $\mathbf{W}(\bar{\mathbf{Q}})$, one obtains the adiabatic energies as a function of \bar{Q}_i .

The two adiabatic potential energy surfaces are computed by diagonalizing the potential energy matrix defined in Eq. (2):

$$U_{A,B}(\bar{\mathbf{Q}}) = \frac{1}{2} \left\{ \lambda_{x_1} \bar{Q}_{x_1} + \lambda_{x_2} \bar{Q}_{x_2} + \sum_{i,j=1}^{3N-6} \frac{\omega_{ij}}{2} \bar{Q}_i \bar{Q}_j \right\} \pm \frac{1}{2} \sqrt{\left[\delta\kappa \bar{Q}_{x_1} + \sum_{i,j=1}^{3N-6} \frac{\delta\gamma_{ij}}{2} \bar{Q}_i \bar{Q}_j \right]^2 + 4 \left[\kappa^{AB} \bar{Q}_{x_2} + \sum_{i,j=1}^{3N-6} \frac{\eta_{ij}^{AB}}{2} \bar{Q}_i \bar{Q}_j \right]^2} \quad (4)$$

As before, the potential energy constants used are defined in Table 1. The difference of the two gradient projections along the non-adiabatic interstate coupling vector, $\delta\kappa_{x_2}$, vanishes as does the $\kappa_{x_1}^{AB}$ term, because the gradient difference [Eq. (3b)] and the non-adiabatic interstate coupling [Eq. (3c)] vectors are chosen perpendicular to one other. For simplicity's sake, we therefore suppress the use of subscripts for the terms $\delta\kappa$ and κ^{AB} .

The physical meaning of Eq. (4) merits a few comments. From Eq. (4), one can see the effect of including second-order potential energy constants, $\delta\gamma_{ij}$ and η_{ij}^{AB} , in the description of conical intersections. Because of these second-order terms, it is clear that the degeneracy is lifted at second order also along the co-ordinates spanning the $(3N-8)$ vectors perpendicular to the branching plane, \bar{Q}_i ($i = 3, 4, \dots, 3N-6$) (i.e., when the branching plane co-ordinates, \bar{Q}_{x_1} and \bar{Q}_{x_2} , are set to zero, the square root does not equal zero at second order). Further, within the first-order description of the intersection space, i.e., along the $(3N-8)$ \bar{Q}_i , the profiles of the two potential energy surfaces resemble those of molecules showing the Renner–Teller effect (see for example [1, 2, 24–26, 34] and references therein).

We now turn our attention to the curvature of the intersection hyper-line energy. Thus, as we have shown above, at second order the degeneracy is lifted along the $(3N-8)$ \bar{Q}_i in addition to the two branching space co-ordinates, $(\bar{Q}_{x_1}, \bar{Q}_{x_2})$. The locus of points along which the degeneracy is retained at second order can be described by a set of *parabolic intersection co-ordinates* (f_i), as described in detail in [24–26]. Our objective now is to express the Hessian in these curvilinear co-ordinates, i.e., to compute the *intersection-space Hessian*. The diagonalization of this intersection-space Hessian gives the signature of the intersection hyper-line energy.

The parabolic intersection co-ordinates are given as:

$$\bar{Q}_{x_1} = \sum_{i,j=3}^{3N-6} \alpha_{ij} f_i f_j \quad \alpha_{ij} = -\frac{{}^{IS}\delta\gamma_{ij}}{2\delta\kappa} \quad (5a)$$

$$\bar{Q}_{x_2} = \sum_{i,j=3}^{3N-6} \mu_{ij} f_i f_j \quad \mu_{ij} = -\frac{{}^{IS}\eta_{ij}^{AB}}{2\kappa^{AB}} \quad (5b)$$

$$\bar{Q}_i = \beta_i f_i \quad \beta_i = 1 \quad (5c)$$

Expressing the energy function [Eq. (4)] as function of these curvilinear co-ordinates, one obtains the energy of the intersection seam as shown in Eq. (6).

$$U_{\text{Seam}} = \frac{1}{2} \left\{ \sum_{i,j \in IS} \lambda_{x_1} (\alpha_{ij} f_i f_j) + \lambda_{x_2} (\mu_{ij} f_i f_j) + \frac{{}^{IS}\omega_{ij}}{2} \beta_i \beta_j f_i f_j \right\} \quad (6)$$

The superscript *IS* is introduced to indicate that the corresponding quantities have been computed by projecting out the two branching plane modes, as proposed in our previous studies [24–26].

The Hessian of the seam energy evaluated in curvilinear co-ordinates at an optimized crossing point, i.e., the *intersection-space Hessian*, is a $(3N-8)$ by $(3N-8)$ matrix and is defined as:

$$\begin{aligned} \left. \frac{\partial^2 U_{\text{Seam}}}{\partial f_i \partial f_j} \right|_{f=0} &= \frac{1}{2} \left({}^{IS}\omega_{ij} \beta_i \beta_j + 2\lambda_{x_1} \alpha_{ij} + 2\lambda_{x_2} \mu_{ij} \right) \\ &= \frac{1}{2} \left({}^{IS}\omega_{ij} - \frac{\lambda_{x_1} {}^{IS}\delta\gamma_{ij}}{\delta\kappa} - \frac{\lambda_{x_2} {}^{IS}\eta_{ij}^{AB}}{\kappa^{AB}} \right) \end{aligned} \quad (7)$$

It should be noticed that in Eq. (7) the indices i and j run from 3 to $3N-6$. The diagonalization of this matrix provides the seam force constants of the molecule at an optimized conical intersection point. As for a single potential energy surface [Eq. (1)], the force constants can be used to compute the curvatures of the intersection seam energy or the frequencies of the molecule in the intersection space. From the diagonalization, a set of eigenvectors is also obtained. These vectors are tangent vectors to the curvilinear intersection co-ordinates, f_i , at the reference point, and they have the same meaning as Q_i discussed for Eq. (1).

It is worth mentioning that using the potential energy constants defined in Table 1, one can also quantify the local

topology of a critical point of conical intersection as *sloped* or *peaked*, using the nomenclature originally proposed by Atchity et al. [16]. However, we note that other ways to classify the local topology of conical intersections have been elsewhere reported (see for example [2]).

$$\sigma_i = [(\lambda_i)^2 - (\delta\kappa_i)^2] \quad i = x_1, x_2 \quad (8)$$

When σ_i is positive then a sloped topology arises, otherwise a peaked topology occurs. We now explain the origin of Eq. (8). A sloped conical intersection arises when the gradients of the two potential energy surfaces point in the same direction. On the other hand, a peaked conical intersection occurs when the gradients of the two intersecting potential energy surfaces are directed towards different directions. Thus, to discriminate peaked conical intersections from sloped conical intersections along the gradient difference vector, for instance, one can use the signs of the gradient projections, $\kappa_{x_1}^A$ and $\kappa_{x_1}^B$. Therefore, since $\text{sign}(\sigma_i) = \text{sign}(\kappa_i^A \cdot \kappa_i^B)$, σ_i can be used to quantify the local topology of conical intersections.

In our first study on the curvature of the intersection seam energy [26], we neglected the second-order non-adiabatic coupling elements, ${}^{IS}\eta_{ij}^{AB}$, and we assumed that the remaining second-order matrix, $\delta\gamma_{ij}$, was diagonal. However, we will show below that Eq. (18) in [26], given as Eq. (9) here, is a limiting case of the new working equation [Eq. (7)]. In other words, we will show that Eq. (9) is the same as Eq. (7) when only the diagonal intra-state coupling terms, $\delta\gamma_{ii}$, are considered, and the second-order interstate coupling constants, ${}^{IS}\eta_{ij}^{AB}$, are set to zero.

$$\left. \frac{\partial^2 U_{\text{Seam}}}{\partial f_i^2} \right|_{f=0} = 2 \left\{ \left(\frac{\gamma_{ii}^A}{{}^{IS}\delta\gamma_{ii}} \right) - \left(\frac{\kappa^A}{\delta\kappa} \right) \right\} \quad (9)$$

If states *A* and *B* are chosen arbitrarily and the curvature of the energy seam needs to be a single value, then the following must hold:

$$\left\{ \left(\frac{\gamma_{ii}^B}{{}^{IS}\delta\gamma_{ii}} \right) - \left(\frac{\kappa^B}{\delta\kappa} \right) \right\} = \left\{ \left(\frac{\gamma_{ii}^A}{{}^{IS}\delta\gamma_{ii}} \right) - \left(\frac{\kappa^A}{\delta\kappa} \right) \right\} \quad (10)$$

Using this equality, rearranging Eq. (9) and using some of the constants defined in Table 1, one obtains:

$$\left. \frac{\partial^2 U_{\text{Seam}}}{\partial f_i^2} \right|_{f=0} = \frac{1}{{}^{IS}\delta\gamma_{ii}} \left\{ {}^{IS}\omega_{ii} - \frac{\lambda_{x_1}}{\delta\kappa} {}^{IS}\delta\gamma_{ii} \right\} \quad (11)$$

Although the elements obtained in Eq. (11) seem different from the diagonal elements of the intersection-space Hessian [Eq. (7)], one should note that in the previous development a $\frac{1}{2}$ factor preceding the second-order term in the Taylor expansion of the potential energy matrix (Eq. (3a) in [26]) was neglected, since the purpose of that study was mainly the sign and not the actual value of the energy seam curvature.

Furthermore, using that parameterization one should have taken into account the scale factors in the differentiation procedure [35]. These factors evaluated at the origin, $f_k = 0$, are equal to one for the parameterization reported in Eq. (5), but they equal $({}^{IS}\delta\gamma_{ii})^{-\frac{1}{2}}$ when computed for the parameterization used in [26]. Thus, if Eq. (11) is multiplied by ${}^{IS}\delta\gamma_{ii}$ and the neglected $\frac{1}{2}$, one re-obtains exactly the same diagonal elements of the intersection-space Hessian reported in Eq. (7). In summary, we have shown that the equation previously obtained for the curvature of the energy seam at an optimized conical intersection is a limiting case of the more general one given here [Eq. (7)] and in [24].

We conclude this section by mentioning that in this paper we will focus only on the intersection space and its description at the second order. However, using Eq. (4), two co-ordinates perpendicular to the second-order intersection space (in the sense proposed by Atchity et al. [16]) can be defined:

$$f_1 = \delta\kappa \bar{Q}_{x_1} + \sum_{i,j=3}^{3N-6} \frac{\delta\gamma_{ij}}{2} \bar{Q}_i \bar{Q}_j = 0 \quad (12a)$$

$$f_2 = \kappa^{AB} \bar{Q}_{x_2} + \sum_{i,j=3}^{3N-6} \eta_{ij}^{AB} \bar{Q}_i \bar{Q}_j \quad (12b)$$

It is intuitively clear that moving away from a conical intersection point along one of the co-ordinates defined above means that the two potential energy surfaces [Eq. (4)] will split apart. Thus these two curvilinear co-ordinates span the *parabolic branching space* [24], and are currently under investigation. It should be noted that the second-order co-ordinates are merely an extension of the corresponding first-order co-ordinates. Indeed if the second-order terms are neglected it can easily be appreciated that f_1 and f_2 correspond to the gradient difference \bar{Q}_{x_1} , and the interstate coupling \bar{Q}_{x_2} , co-ordinates, respectively.

3 Computational details

All of the conical intersection critical points for fulvene were computed and optimized using the *complete active space self-consistent field* (CASSCF) method implemented in a development version of Gaussian [36]. An active space of six π electrons and six π orbitals, [CAS(6,6)], with the Dunning cc-pVDZ basis set was used. Although this active space was selected to describe the π interactions, it is also capable of describing the σ bond elongation present in some of the optimized structures satisfactorily, as we shall show in the next section. In the case of **CIplan**, for instance, we found that the inclusion of two more electrons and orbitals (one σ and one σ^*) in the active space leads to a variation of only 0.2

Angstroms in the length of the exocyclic CC bond. Therefore, the (6,6) active space is sufficient to analyse the S_0/S_1 crossing seam of fulvene.

Each of the conical intersection points was optimized using the algorithm proposed by Bearpark et al. [19] and state-averaged wavefunctions for equally weighted ground and first excited states. Moreover, an accuracy of 10^{-10} on the electronic energy was imposed such that an energy difference of less than $0.05 \text{ kcal mol}^{-1}$ was reached at each of the degenerate points.

Throughout the rest of this paper, we will refer to the un-mass-weighted Cartesian eigenvectors obtained from the diagonalization of the intersection-space Hessian [Eq. (7)] as the *seam normal modes*. The eigenvalues obtained from the same diagonalization can be expressed in cm^{-1} giving what we will refer to as the *seam frequencies*. First- and second-order potential energy constants as well as the seam frequencies and seam normal modes were computed using the algorithm reviewed in the previous section (A more detailed discussion on the computation of the potential energy constants can be found in [24] and [26]) and implemented in a development version of Gaussian. It should be emphasized that once one can compute the state-averaged Hessians for the two potential energy surfaces, implementation of the intersection-space Hessian [Eq. (7)] is relatively straightforward.

If an imaginary seam frequency was computed, then the corresponding seam normal mode was used to detect lower energy structures on the crossing seam: starting from the optimized conical intersection structure, a displacement along this vector was taken to generate the new geometry, from which a new conical intersection optimization was performed. A full reaction path computation restricted to the intersection space would be required to infer rigorously that two conical intersection geometries are both on the same seam. Nevertheless, the procedure adopted here strongly suggests that two geometries (initial and final) are connected along the crossing hyper-line, which is the main purpose of this study. Furthermore, through constrained optimizations [21], we have already shown in another way that two of the seam critical points we discuss below lie on the same seam.

4 Results and discussions

Analysis of the intersection-space Hessian [Eq. (7)] has been used to gain additional insights into the S_0/S_1 intersection seam of the fulvene molecule. The main purpose of this paper is to show how optimized conical intersection geometries can be characterized as minima or saddle points on the intersection hyper-line by using the intersection-space Hessian. In this work—for the first time for fulvene—we have computed the eigenvectors of the intersection-space Hessian; not just

the eigenvalues as in [26]. Thus we are now able to discuss the connectivity of all of the optimized conical intersection geometries using the eigenvectors of the intersection-space Hessian: each saddle point can be linked to a lower energy structure by following eigenvectors corresponding to imaginary frequencies.

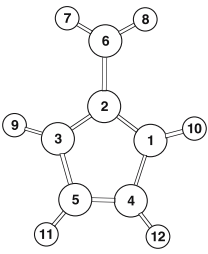
Fulvene is one of the isomers of benzene and its first excited state is characterized by a lack of fluorescence indicating a fast internal conversion to the ground state *via* a conical intersection. Previous CASSCF studies on the fulvene S_0/S_1 intersection seam located four different conical intersection geometries, namely **CI₆₃**, **CI_{Pyr}**, **CI_{Perp}** and **CI_{Plan}** [21,26–29]. These four structures were previously characterized by a more approximate second-order analysis. As we will see, the nature of these critical points (number of imaginary frequencies) now changes, and an additional conical intersection geometry has been optimized, using the new insights provided by having both eigenvectors and eigenvalues of the intersection-space Hessian.

The geometries and energies of the five conical intersection (CI) structures **CI₆₃**, **CI_{Pyr}**, **CI_{Perp}**, **CI_{Plan}** and **CI_{Min}**, are reported in Table 2, and all but **CI_{Min}** are in agreement with the ones previously reported in the literature [21,26–29].

The seam frequency analysis reveals that the four previously reported structures (i.e., **CI₆₃**, **CI_{Pyr}**, **CI_{Perp}**, **CI_{Plan}**) are either first- or second-order saddle points (Table 4) in the intersection space. At each of these optimized points, first-order branching plane (i.e., gradient difference and non-adiabatic interstate coupling) vectors (Table 3) and the seam normal modes (Table 4) were computed. Moreover, whenever an imaginary frequency was computed, the corresponding seam normal mode was used to detect lower-lying conical intersection points as discussed in the previous section. We have consequently located an additional conical intersection point, **CI_{Min}** (Table 2), which appears to be the global minimum on the intersection hyper-line.

In Fig. 1, we show the topology of the conical intersection seam geometries computed on the S_0/S_1 seam of fulvene. Torsion and pyramidalization motions of the methylenic group [8,10,21,26–29] are the most important modes involved in the description of this intersection seam. For the structures studied, these two modes are orthogonal to the two motions defining the branching plane and therefore they are two of the $(3N-8)$ vectors describing the intersection space at the first order. In the first-order description of conical intersections, if one takes a finite step within the intersection space, the degeneracy between the two states is lifted.

In the second-order description of conical intersections, the intersection space is curved and if one takes a step in curvilinear co-ordinates, the degeneracy is retained. The eigenvectors, which are combinations of the pyramidalization and torsion modes and those belonging to the branching

Table 2 Conical intersection critical points optimized for fulvene


	CI_{Min} C ₁	CI₆₃ C ₂	CI_{Perp} C _{2v}	CI_{Pyr} C _s	CI_{Plan} C _{2v}
Energy (Hartree)	−230.6513957 ^a	−230.6513918 ^a	−230.64783	−230.63543	−230.63545
Relative energy (kcal mol ^{−1})	0.0	0.003	2.3	8.3	9.7
$R(1,2) = R(2,3)$	1.410	1.409	1.424	1.377	1.372
$R(1,4)$	1.461	1.461	1.424	1.521	1.531
$R(3,5)$	1.460	1.461	1.424	1.521	1.531
$R(4,5)$	1.371	1.371	1.413	1.326	1.320
$R(2,6)$	1.481	1.482	1.478	1.567	1.578
$R(6,7) = R(6,8)$	1.081	1.081	1.082	1.084	1.078
$R(3,9) = R(1,10)$	1.080	1.079	1.079	1.081	1.082
$R(4,12) = R(5,11)$	1.079	1.079	1.079	1.079	1.079
$D(7,6,2,3)$	−58.69	−63.14	90.0	−18.06	0.0
$D(7,6,2,8)$	171.30	180.00	90.0	180.00	180.00

The bond lengths and angles are reported in angstroms and degrees, respectively

^a The calculations were carried out with an accuracy of 10^{-10} on the electronic energy

plane (skeletal deformations), are tangent to these curvilinear co-ordinates. Accordingly, a step along one of the curvilinear co-ordinates corresponding to these eigenvectors keeps the molecule in the second-order intersection space [as shown in Eq. (5)] and simultaneously lowers the energy. For example, moving away from the **CI_{Plan}** geometry, which is a second-order saddle point within the intersection space (Table 4), and following the positive direction of the two modes reported by dotted lines in Fig. 1, i.e., the motions corresponding to the two imaginary frequencies (Table 4), one reaches the **CI_{Pyr}** and **CI₆₃** structures. This situation is analogous to a second-order saddle point on a single potential energy surface, except that the motion is along a curvilinear co-ordinate, which keeps one in the intersection space. We now develop this idea along some of the other connecting lines in Fig. 1.

Along the curvilinear co-ordinate connecting **CI_{Plan}** to **CI₆₃**, there exists another critical point on the S_0/S_1 crossing hyper-line: **CI_{Perp}** (Table 2), not shown in Fig. 1. We emphasize that the curved nature of the intersection seam co-ordinate is a central feature of the analysis. For example, starting from **CI_{Plan}** the curvilinear co-ordinate that connects it to **CI₆₃** is a non-linear combination of an intersection space mode (i.e., torsion corresponding to the imaginary frequency in Table 4), and branching space motions (i.e., bond stretch-

ing in Table 3). Thus, the intersection space is not rectilinear as predicted by the first-order description of this space, and the intersection space co-ordinate corresponding to the torsion motion alone does not connect the two isomers.

Similarly, starting from the **CI_{Pyr}** geometry, a rotational motion, i.e., seam mode corresponding to the imaginary frequency at $392i \text{ cm}^{-1}$ (Table 4), combined with branching space motions (Table 3) leads to the **CI_{Min}** structure. The same result is achieved taking a small displacement from **CI₆₃** along the pyramidalisation vector, which corresponds to the seam normal mode associated with the imaginary frequency computed (Table 4), followed by a conical intersection optimization. Therefore, these results suggest that both the geometries **CI_{Pyr}** and **CI₆₃** are saddle points connected by the valley where **CI_{Min}** lies.

We now consider the analysis of the local topology (sloped vs. peaked) at various conical intersection critical points using Eq. (8). From an inspection of Table 5, it is clear that the planar and pyramidalized conical intersections (**CI_{Plan}** and **CI_{Pyr}**) are sloped and the remaining conical intersections are peaked. For sloped conical intersections, the excited- and ground-state local minima along a cross-section in the branching space lie on the same side of the conical intersection geometry. In contrast, for a peaked conical intersection, the two minima lie on the two different sides of the conical

Table 3 Gradient difference and interstate coupling vectors at the critical points on the fulvene conical intersection seam shown in Table 2

Geometry	Gradient difference vector	Interstate coupling vector
CI_{Plan}		
CI_{Perp}		
CI_{63}		
CI_{Min}		
CI_{Pyr}		

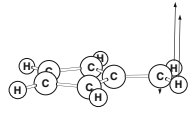
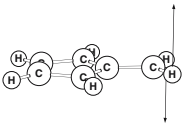
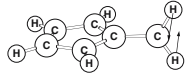
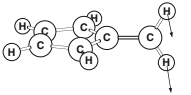
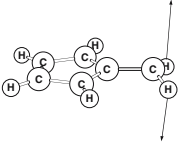
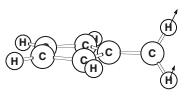
intersection point. Thus the change in the local topology is a further diagnostic of the curved nature of the intersection space, as discussed in [21].

The second-order analysis just presented enables us to discuss conjectures about the extended nature of the conical intersection seam in the calculations of other workers. Deeb et al. [28] have suggested that CI_{plan} and CI_{perp} belong to two different S_0/S_1 intersection seams, based on the fact that in their calculation, the degeneracy at CI_{plan} along the torsion co-ordinate is only preserved for angles larger than 45° . In fact (Table 4), CI_{plan} is a second-order saddle point, where one of the directions of negative curvature is the torsion that

(partly) leads to CI_{perp} . The lifting of the degeneracy along the torsion is an artifact of using a first-order representation. When one allows mixing of the intersection and branching spaces (described at the first order), the degeneracy can be maintained along the resulting curvilinear co-ordinate. So, this conjecture of Deeb et al. is incorrect and an artefact of using a first-order approximation of the intersection space.

Deeb et al. also suggested that CI_{plan} is involved in a bond breaking process, inferred from the fact that the exocyclic CC bond is stretched to approximately 1.7\AA at the CAS(8,8)/cc-pVDZ level of theory. In fact, the gradient difference vector [shown in Table 3 for CAS(6,6)] involves a CC stretch.

Table 4 Imaginary frequencies evaluated at the critical points on the fulvene conical intersection seam shown in Table 2 ($i = \sqrt{-1}$)

Geometry	Seam frequency (cm^{-1})	Symmetry ^a	Intersection space modes
$CI_{Plan}(C_{2v})$	591 <i>i</i>	b_1	
$CI_{Plan}(C_{2v})$	437 <i>i</i>	a_2	
$CI_{Perp}(C_{2v})$	612 <i>i</i>	a_2	
$CI_{Perp}(C_{2v})$	127 <i>i</i>	b_2	
$CI_{Pyr}(C_s)$	392 <i>i</i>	a'	
$CI_{63}(C_2)$	73 <i>i</i>	b	

^a The symmetry of the normal mode is given within the point group of the geometry it belongs to

However, at CI_{Plan} one has a sloped topology at both levels of theory (Table 5), and the excited B_2 state has a positive gradient along the CC stretching co-ordinate (see also Fig. 4 of [26]). Thus, the potential energy along the stretching co-ordinate is “bound” and not “repulsive” as one would expect for a state that leads to scission of this CC bond.

To conclude, we briefly compare the results presented here with the more approximate implementation described in [26]. The major point of difference is that the CI_{63} geometry was previously predicted to be a minimum [26] and the lowest energy point on the fulvene S_0/S_1 conical intersection seam. However, in Table 4, one can see that CI_{63} is in fact a first-order saddle point within the inter-

section space. This result was also confirmed by locating a marginally ($<0.01 \text{ kcal mol}^{-1}$) lower energy structure on the same intersection seam, CI_{Min} (Table 2). It is quite difficult to make a detailed comparison between the approximate results presented in [26] and our new results, because in [26] we needed to manually match up eigenvectors resulting from independent diagonalizations of the *state A* and *state B* Hessians, which was often quite difficult. (Nevertheless, these first results were sufficiently interesting that they stimulated the present work.) Other minor differences include CI_{Perp} , which changes from a first- to a second-order saddle point, and CI_{Pyr} , which changes from a minimum to a first-order saddle point.

Fig. 1 Schematic representation of the conical intersection hyper-line topology (excluding CI_{Perp}) in the space of torsion and pyramidalization. The seam normal modes corresponding to the imaginary frequencies that connect the conical intersection geometries optimized on the S_0/S_1 seam of fulvene are shown as vectors for hydrogen motions only

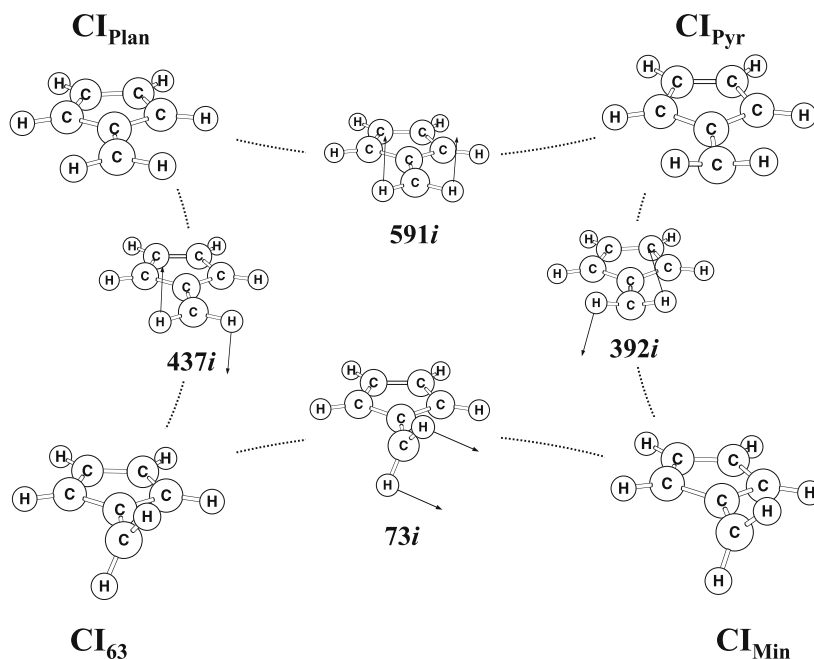


Table 5 First-order potential constant values/(a.u) at the conical intersection critical points for fulvene (Table 2)

Geometry	κ^{AB}	$\delta\kappa$	λ_1	λ_2	σ_{x_1}	Topology
CI_{Plan}	0.115	0.261	0.516	0.000	0.198	Sloped
CI_{Perp}	0.114	0.229	-0.020	0.000	-0.052	Peaked
CI_{Pyr}	0.114	0.263	-0.475	0.000	0.156	Sloped
CI_{63}	0.109	0.245	0.192	0.000	-0.023	Peaked
CI_{Min}	0.121	0.223	0.080	0.174	-0.043	Peaked
CI_{Plan}^a	0.118	0.245	-0.465	0.267	0.156	Sloped

^a Computed with CASSCF(8,8) level of theory

5 Conclusions

In this paper we report a comprehensive picture of the S_0/S_1 extended conical intersection seam of fulvene using a second-order description. An additional seam critical point (CI_{Min}) has been found and shown to be the global minimum. The previously reported [21, 26–29] CI_{Plan} and CI_{Perp} are second-order saddle points, and the previously documented CI_{63} and CI_{Pyr} are first-order saddle points on the $(3N-8)$ dimensional intersection hyper-line.

These results are consistent with previous studies where the torsion and pyramidalization modes were proven to be particularly important for the analysis of the intersection seam of fulvene. However, they differ from the conclusion drawn by Deeb et al. [28]. The present results (together with [21]) strongly suggest that all of the conical intersection critical points are interconnected on the same seam, in contrast to

the suggestion of Deeb et al. that there may be two different seams of intersection.

Acknowledgments All the calculations were carried out with EPSRC-funded computers. One of the authors (L. B.) is financed by the Spanish Ministerio de Educación y Ciencia for Project No. CTQ2005-04563 and the Ramón y Cajal program. F.S. is supported by a student-ship granted by Gaussian Inc.

References

- Yarkony DR (1996) Rev Mod Phys 68:985
- Yarkony DR (2004) Conical intersections: their description and consequences. In: Domcke W, Yarkony DR, Koppel H (eds) Conical intersections: electronic structure, dynamics and spectroscopy. World Scientific, Singapore, p 127
- Migani A, Olivucci M (2004) Conical intersections and organic reaction mechanisms. In: Domcke W, Yarkony DR, Koppel H (eds) Conical intersections: electronic structure, dynamics and spectroscopy. World Scientific, Singapore, p 271
- Olivucci M, Robb MA, Bernardi F (2000) Calculations of excited state conformational properties. In: Waluk J (ed) Calculations of excited state conformational properties. Wiley-VCH, New York, p 297
- Robb MA, Garavelli M, Olivucci M, Bernardi F (2000) A computational strategy for organic photochemistry. In: Lipkowitz KB, Boyd DB (eds) Reviews in computational chemistry, vol 15. Wiley-VCH, New York, p 87
- Bernardi F, Olivucci M, Robb MA (1996) Chem Soc Rev 25:321
- Garavelli M (2006) Theor Chem Acc 116:87
- Klessinger M, Michl J (1995) Excited states and photochemistry of organic molecules. Wiley-VCH, New York
- Toniolo A, Levine B, Thompson A, Quenneville J, Ben-Nun M, Owens J, Oisen S, Manohar L, Martinez TJ (2005) Photochemistry from first principles and direct dynamics. In: Kutateladze A (ed) Computational methods in organic photochemistry. Marcel-Dekker, New York

10. Michl J, Bonacic-Koutecky V (1990) *Electronic aspects of organic photochemistry*. Wiley-VCH, New York
11. Applegate BE, Barckholtz TA, Miller TA (2003) *Chem Soc Rev* 32:38
12. Koppel H, Domcke W, Cederbaum LS (2004) The multi-mode vibronic coupling approach. In: Domcke W, Yarkony DR, Koppel H (eds) *Conical intersections: electronic structure, dynamics and spectroscopy*. World Scientific, Singapore, p 323
13. Worth GA, Meyer HD, Cederbaum LS (2004) Multidimensional dynamics involving a conical intersection: wavepacket calculations using the MCTDH method. In: Domcke W, Yarkony DR, Koppel H (eds) *Conical intersections: electronic structure, dynamics and spectroscopy*. World Scientific, Singapore, p 583
14. Jasper AW, Kendrick BK, Mead CA, Truhlar DG (2004) Non-Born-oppenheimer chemistry: potential surfaces, couplings, and dynamics. In: Yang X, Liu K (eds) *Modern trends in chemical reaction dynamics: experiments and theory (Part 1)*. World Scientific, Singapore, p 329
15. Bersuker IB (2006) *The Jahn-Teller effect*. Cambridge University Press, Cambridge
16. Atchity GJ, Xantheas SS, Ruedenberg K (1991) *J Chem Phys* 95:1862
17. Toniolo A, Ben-Nun M, Martinez TJ (2002) *J Phys Chem A* 106:4679
18. Serrano-Andres L, Merchan M, Lindh R (2005) *J Chem Phys* 122:104107
19. Bearpark MJ, Robb MA, Schlegel HB (1994) *Chem Phys Lett* 223:269
20. Yarkony DR (2004) Determination of potential energy surface intersections and derivative couplings in the adiabatic representation. In: Domcke W, Yarkony DR, Koppel H (eds) *Conical intersections: electronic structure, dynamics and spectroscopy*. World Scientific, Singapore, p 129
21. Bearpark MJ, Blancafort L, Paterson MJ (2006) *Mol Phys* 104:1033
22. Yarkony DR (2005) *J Chem Phys* 123:134106
23. Yarkony DR (2005) *J Chem Phys* 123:204101
24. Sicilia F, Bearpark MJ, Blancafort L, Robb MA (2007) *J Phys Chem A* 111:2182
25. Paterson MJ, Bearpark MJ, Robb MA, Blancafort L, Worth GA (2005) *Phys Chem Chem Phys* 7:2100
26. Paterson MJ, Bearpark MJ, Robb MA, Blancafort L (2004) *J Chem Phys* 121:11562
27. Dreyer J, Klessinger M (1994) *J Chem Phys* 101:10655
28. Deeb O, Cogan S, Zilberg S (2006) *Chem Phys* 325:251
29. Bearpark MJ, Bernardi F, Olivucci M, Robb MA, Smith BR (1996) *J Am Chem Soc* 118:5254
30. Boggio-Pasqua M, Bearpark MJ, Ogliaardo F, Robb MA (2006) *J Am Chem Soc* 128:1053
31. Mead CA (1983) *J Chem Phys* 78:807
32. Wilson Jr EB, Decius JC, Cross PC (1980) *Molecular vibrations*. Dover, New York
33. Cederbaum LS, Koppel H, Domcke W (1981) *Int J Q Chem* 251
34. Lee TJ, Fox DJ, Schaefer III HF, Pitzer RM (1984) *J Chem Phys* 81:356
35. Byron FW, Fuller RW (1969) *Mathematics of classical and quantum physics*. Dover Publications, Inc., New York
36. Gaussian Development Version, Revision E05, Frisch MJ, Trucks GW, Schlegel HB, Scuseria GE, Robb MA, Cheeseman JR, Montgomery Jr JA, Vreven T, Kudin KN, Burant JC, Millam JM, Iyengar SS, Tomasi J, Barone V, Mennucci B, Cossi M, Scalmani G, Rega N, Petersson GA, Nakatsuji H, Hada M, Ehara M, Toyota K, Fukuda R, Hasegawa J, Ishida M, Nakajima T, Honda Y, Kitao O, Nakai H, Klene M, Li X, Knox JE, Hratchian HP, Cross JB, Bakken V, Adamo C, Jaramillo J, Gomperts R, Stratmann RE, Yazyev O, Austin AJ, Cammi R, Pomelli C, Ochterski JW, Ayala PY, Morokuma K, Voth GA, Salvador P, Dannenberg JJ, Zakrzewski VG, Dapprich S, Daniels AD, Strain MC, Farkas O, Malick DK, Rabuck AD, Raghavachari K, Foresman JB, Ortiz JV, Cui Q, Baboul AG, Clifford S, Cioslowski J, Stefanov BB, Liu G, Liashenko A, Piskorz P, Komaromi I, Martin RL, Fox DJ, Keith T, Al-Laham MA, Peng CY, Nanayakkara A, Challacombe M, Gill PMW, Johnson B, Chen W, Wong MW, Gonzalez C, Pople JA (2006) Gaussian, Inc, Wallingford CT